CHEMISTRY OF MATERIALS
Article

Chem. Mater. **2009,** *21,* 5819–5825 5819
DOI:10.1021/cm902379x

Dye-Condensed Biopolymeric Hybrids: Chromophoric Aggregation and Self-Assembly toward Fluorescent Bionanoparticles for Near Infrared Bioimaging

Chang-Keun Lim,[†] Sehoon Kim,*[,†] Ick Chan Kwon,[†] Cheol-Hee Ahn,*[,‡] and Soo Young Park*[,‡]

[†]*Biomedical Research Center, Korea Institute of Science and Technology, 39-1 Hawolgok-dong, Seongbuk-gu, Seoul 136-791, Korea and* [‡]*Department of Materials Science & Engineering, Seoul National University, San 56-1, Shillim-dong, Kwanak-gu, Seoul 151-744, Korea*

Received August 3, 2009. Revised Manuscript Received November 5, 2009

Novel fluorescent bionanoparticles (GC3CN*x*) were prepared by self-assembly of biopolymeric amphiphiles that are composed of hydrophilic glycol chitosan (GC) as a biopolymeric backbone and a dipolar tricyanostilbene derivative (3CN) as a densely conjugated hydrophobic pendant. In the molecular design of 3CN, a dipolar electronic structure was introduced to spectrally shift the aggregation-induced enhanced fluorescence of the α-cyanostilbene skeleton toward the near-infrared (NIR) useful for bioimaging. It has been found that the fluorescence of GC3CN*x* nanoparticles is red-shifted and intensified by increasing the 3CN content in the biopolymeric amphiphile. By cellular and in vivo imaging experiments, we demonstrate that GC3CN*x* nanoparticles have great potential for NIR bioimaging, with attractive properties including enhanced fluorescence signal, efficient cellular uptake, and better spectral coincidence with the in vivo transparent window.

1. Introduction

Optical bioimaging is one of the biggest growth areas in biological and biomedical research.[1,2] The visualization technology based on the interaction between light and biological matters has been greatly advanced with the availability of various natural and synthetic fluorescent probe molecules.[3,4] Fluorescent nanoparticles are a new generation of imaging probes with attractive capabilities that are superior to those of molecular counterparts. Their advantages include enhanced cell permeability, passive tumor targeting by the enhanced permeability and retention (EPR) effect, surface engineering for multiple bioconjugation, and targeted delivery of therapeutic payloads.[4−7] Among various kinds of nanoprobes, polymeric nanoparticles concentrated with dyes exhibiting aggregation-induced enhanced emission (AIEE) are newly emerging candidates that are potentially promising for the advanced imaging applications demanding intense fluorescence signal.[8,9] AIEE is a unique phenomenon occurring in a special class of dyes that are less fluorescent in solution but show great enhancement of emission by solidification,[10] as opposed to the fluorescence quenching of common organic dyes in the concentrated or aggregated states.[11] Conceptually, the fluorescence signal output from individual nanoparticles is proportional to the product of fluorescence efficiency and loading density of the embedded dyes. Consequently, it can be boosted by raising the loading amount of fluorescence-retaining AIEE-active dyes, whereby a signal breakthrough of nanoprobes can be achieved in a form of dye-concentrated nanoparticles.[8]

Proper choice of the particulate matrix material is of another importance to produce high-performance

*Address correspondence to either author. E-mail: sehoonkim@kist.re.kr (S.K.); chahn@snu.ac.kr (C.-H.A.); parksy@snu.ac.kr (S.Y.P.).

(1) Weissleder, R.; Pittet, M. J. *Nature* **2008**, *452*, 580–589.
(2) Prasad, P. N. *Introduction to Biophotonics*; Wiley: Hoboken, NJ, 2003.
(3) Zhang, J.; Campbell, R. E.; Ting, A. Y.; Tsien, R. Y. *Nat. Rev. Mol. Cell Biol.* **2002**, *3*, 906–918.
(4) Resch-Genger, U.; Grabolle, M.; Cavaliere-Jaricot, S.; Nitschke, R.; Nann, T. *Nat. Methods* **2008**, *5*, 763–775.
(5) Kim, J.-H.; Park, K.; Nam, H. Y.; Lee, S.; Kim, K.; Kwon, I. C. *Prog. Polym. Sci.* **2007**, *32*, 1031–1053.
(6) Cai, W.; Chen, X. *Small* **2007**, *3*, 1840–1854.
(7) Park, K.; Lee, S.; Kang, E.; Kim, K.; Choi, K.; Kwon, I. C. *Adv. Funct. Mater.* **2009**, *19*, 1553–1566.
(8) (a) Kim, S.; Pudavar, H. E.; Bonoiu, A.; Prasad, P. N. *Adv. Mater.* **2007**, *19*, 3791–3795. (b) Kim, S.; Huang, H.; Pudavar, H. E.; Cui, Y.; Prasad, P. N. *Chem. Mater.* **2007**, *19*, 5650–5656. (c) Kim, S.; Ohulchansky, T. Y.; Pudavar, H. E.; Pandey, R. K.; Prasad, P. N. *J. Am. Chem. Soc.* **2007**, *129*, 2669–2675.
(9) (a) Chan, C. P.-Y.; Haeussler, M.; Tang, B. Z.; Dong, Y.; Sin, K.-K.; Mak, W.-C.; Trau, D.; Seydack, M.; Renneberg, R. *J. Immunol. Methods* **2004**, *295*, 111–118. (b) Kim, H.-J.; Lee, J.; Kim, T.-H.; Lee, T. S.; Kim, J. *Adv. Mater.* **2008**, *20*, 1117–1121.
(10) (a) Luo, J.; Xie, Z.; Lam, J. W. Y.; Cheng, L.; Chen, H.; Qiu, C.; Kwok, H. S.; Zhan, X.; Liu, Y.; Zhu, D.; Tang, B. Z. *Chem. Commun.* **2001**, 1740–1741. (b) An, B.-K.; Kwon, S.-K.; Jung, S.-D.; Park, S. Y. *J. Am. Chem. Soc.* **2002**, *124*, 14410–14415. (c) Xiao, D.; Xi, L.; Yang, W.; Fu, H.; Shuai, Z.; Fang, Y.; Yao, J. *J. Am. Chem. Soc.* **2003**, *125*, 6740–6745. (d) Kim, S.; Zheng, Q.; He, G. S.; Bharali, D. J.; Pudavar, H. E.; Baev, A.; Prasad, P. N. *Adv. Funct. Mater.* **2006**, *16*, 2317–2323. (e) Zeng, Q.; Li, Z.; Dong, Y.; Di, C.; Qin, A.; Hong, Y.; Zhu, Z.; Jim, C. K. W.; Yu, G.; Li, Q.; Li, Z. A.; Liu, Y.; Qin, J.; Tang, B. Z. *Chem. Commun.* **2007**, 70–72.(f) Hong, Y.; Lam, J. W. Y., Tang, B. Z. Chem. Commun. **2009**, DOI: 10.1039/b904665h. (g) An, B.-K.; Gihm, S. H.; Chung, J. W.; Park, C. R.; Kwon, S.-K.; Park, S. Y. *J. Am. Chem. Soc.* **2009**, *131*, 3950–3957.
(11) Birks, J. B. *Photophysics of Aromatic Molecules*; Wiley: London, 1970.

Published on Web 11/24/2009

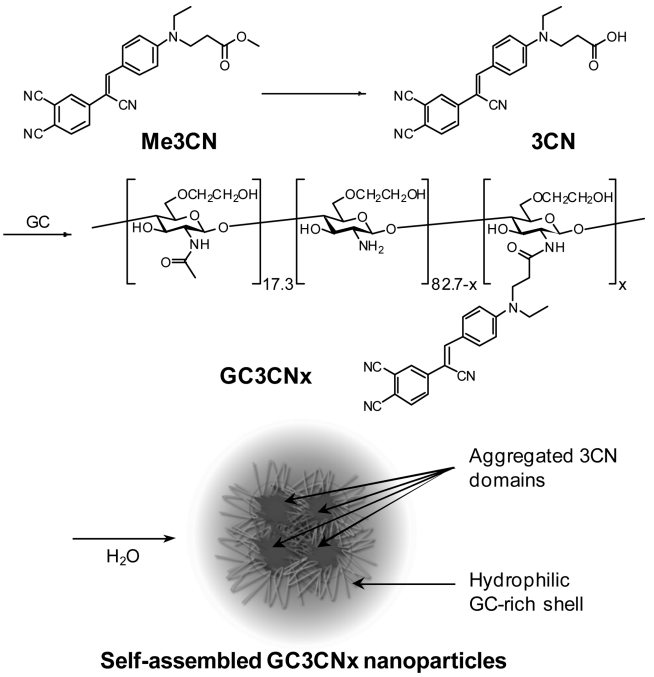

Figure 1. Schematic representation of AIEE-active α-cyanostilbenes (Me3CN and 3CN) and hybrid bionanoparticles implemented therewith (GC3CN*x*), where the feed ratio (*x*) varies from 5 to 83 mol %.

nanoprobes suitable for imaging applications in cells and in vivo. In this context, modified amphiphilic biomacromolecules with an appropriate hydrophilic/hydrophobic balance present outstanding properties:[12,13] (1) high biocompatibility, (2) self-assembled formation of water-dispersed nanoparticles with a characteristic structure comprising a hydrophilic shell and hydrophobic multicores, (3) efficient cellular uptake with less cytotoxicity, (4) prolonged blood circulation to manifest the EPR effect, and (5) lots of reactive functional groups available for further bioconjugation. In our previous reports, it has been shown that hydrophobically modified glycol chitosan is a representative example exhibiting all these advantageous features in a self-assembled nanoparticulate formulation.[13]

In this study, we have designed a novel type of hybrid nanoprobes, to combine the above optical and biorelated advantages in self-assembled biopolymeric nanoparticles. As depicted in Figure 1, the designed bioplymeric amphiphiles (GC3CN*x*) are composed of water-soluble glycol chitosan (GC) and a dipolar tricyanostilbene derivative (3CN) as a densely conjugated hydrophobic pendant. In the structure of 3CN, the central α-cyanostilbene is an AIEE-active skeleton,[10b,g] to the opposite ends of which electron-donating (4-dialkylamino) and accepting (3′, 4′-dicyano) groups were substituted. The resulting dipolar electronic structure was introduced to red-shift the aggregate fluorescence toward the near-infrared (NIR) that is a spectral window with less photon-limiting interferences (absorption, scattering, and autofluorescence) occurring in biological matters.[2] Here we present the synthesis, AIEE characteristics, and nanoparticle formation of GC3CN*x*, along with the demonstration of potentials for bioimaging in cells and in vivo.

2. Results and Discussion

A methyl ester-blocked form of 3CN (Me3CN) was prepared by Knoevenagel condensation between an 4-aminobenzaldehyde derivative and 3,4-dicyanobenzyl cyanide in the presence of piperidine and acetic acid (Scheme 1). The purified Me3CN showed the typical AIEE characteristics: the molecularly isolated state in a good solvent (THF) is nonfluorescent, whereas its solids (water-dispersed nanoaggregates and bulk crystals) have bright fluorescence emissions that are clearly seen in a NIR-filtered imaging system as well as by naked eye under the illumination at 365 nm (Figure 2a). The aggregation-induced change of optical properties was assessed with a suspension of Me3CN nanoaggregates in THF/water (1/9 by vol.), prepared by a simple precipitation method.[14] By nanoaggregation, the monotonic solution absorption at 443 nm was shifted to 472 nm with a hypochromic effect in intensity and an appearance of a new longer-wavelength shoulder at ca. 500 nm (Figure 2b). The fluorescence showed a similar spectral red shift (Figure 2c) and was intensified with a significant increase in the quantum yield from 0.001 (solution) to 0.05 (nanoaggregates). As shown in figure 2b, the aggregate fluorescence has an excitation spectrum similar to the aggregate absorption except the intensified contribution of longer-wavelength components. This indicates that both the red-shifted absorption and the newly appeared shoulder are the main transition pathways to emitting species in nanoaggregates. The observed spectral shift is attributed presumably to the torsion-locking planarization of the distorted solution geometry of Me3CN by aggregation, which narrows the optical bandgap by lengthening the effective π-electron conjugation. Semiempirical calculation and molecular dynamics demonstrated that the geometry of a single Me3CN molecule is severely distorted and free to twist, offering an efficient nonradiative decay pathway in the isolated solution state (see Supporting Information (SI) Figure S1). Accordingly, the restricted intramolecular rotation by aggregation is a plausible reason for the fluorescence enhancement.[10e,f] The appearance of a longer-wavelength absorption shoulder suggests that close stacking of the planarized Me3CN molecules is possibly accompanied with fluorescence-enhancing J-type π-aggregation, often

(12) Janes, K. A.; Calvo, P.; Alonso, M. *J. Adv. Drug. Delivery Rev.* **2001**, *47*, 83–97.
(13) (a) Kim, K.; Kwon, S.; Park, J. H.; Chung, H.; Jeong, S. Y.; Kwon, I. C. *Biomacromolecules* **2005**, *6*, 1154–1158. (b) Lee, M.; Cho, Y. W.; Park, J. H.; Chung, H.; Jeong, S. Y.; Choi, K.; Moon, D. H.; Kim, S. Y.; Kim, I.-S.; Kwon, I. C. *Colloid Polym. Sci.* **2006**, *284*, 506–512. (c) Park, K.; Kim, J.-H.; Nam, Y. S.; Lee, S.; Nam, H. Y.; Kim, K.; Park, J. H.; Kim, I.-S.; Choi, K.; Kim, S. Y.; Kwon, I. C. *J. Controlled Release* **2007**, *122*, 305–314. (d) Nam, H. Y.; Kwon, S. M.; Chung, H.; Lee, S.-Y.; Kwon, S.-H.; Jeon, H.; Kim, Y.; Park, J. H.; Kim, J.; Her, S.; Oh, Y.-K.; Kwon, I. C.; Kim, K.; Jeong, S. Y. *J. Controlled Release* **2009**, *135*, 259–267.
(14) Kasai, H.; Nalwa, H. S.; Okada, S.; Oikawa, H.; Nakanish, H. *Handbook of Nanostructured Materials and Nanotechnology*, Chapter 8.; Academic: New York, 2000; Vol. *5*.

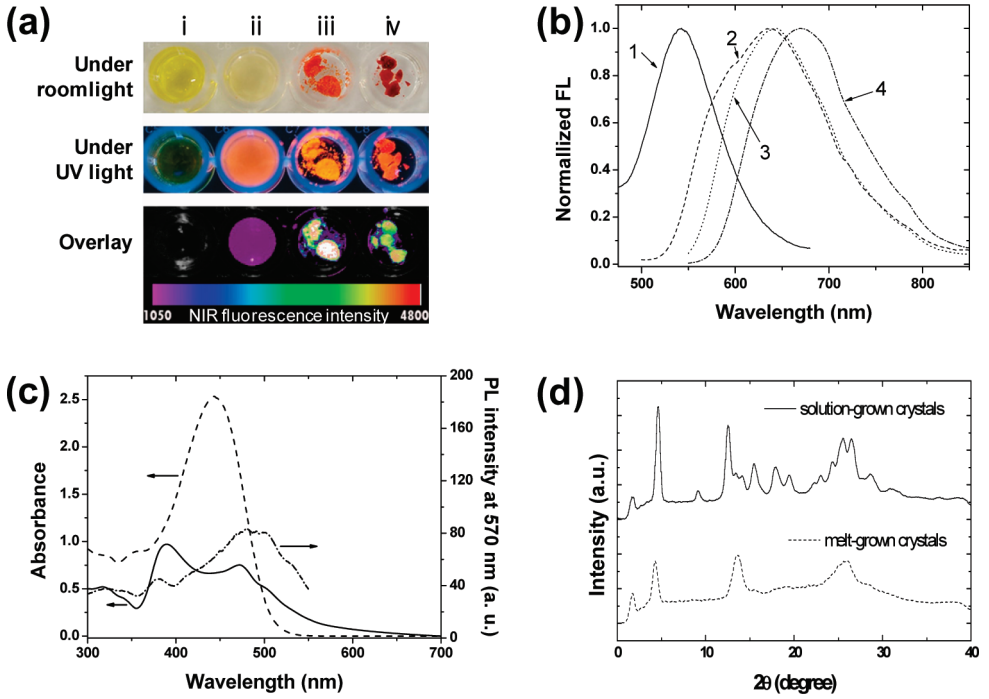

Figure 2. (a) Photographs of Me3CN: (i) THF solution, (ii) nanoparticle dispersion in THF/water (1/9 by vol.), (iii) MeOH-grown crystals, and (iv) melt-grown crystals. True-color optical and fluorescence views under room light and the 365 nm illumination by a hand-held UV lamp were taken with a general-purpose digital camera. Overlay of optical and NIR-filtered fluorescence (680−720 nm) images was taken by a Kodak imaging system with a filter set of TRITC (ex)/Cy5.5 (em). (b) Normalized fluorescence (FL) spectra of Me3CN: (1) THF solution, (2) nanoparticle dispersion in THF/water (1/9 by vol.), (3) MeOH-grown crystals, and (4) melt-grown crystals. The Me3CN concentrations in solution and nanoparticle dispersion were kept at 2×10^{-5} M. (c) Absorption spectra of Me3CN solution in THF (dashed) and nanoparticle dispersion in THF/water (1/9 by vol.) (solid), along with an excitation spectrum for aggregate fluorescence at 570 nm (dash-dotted). (d) Powder X-ray diffractograms of Me3CN crystals grown from a MeOH solution (solid) and from an isotropic melt (dashed).

Scheme 1. Synthetic Route of Me3CN

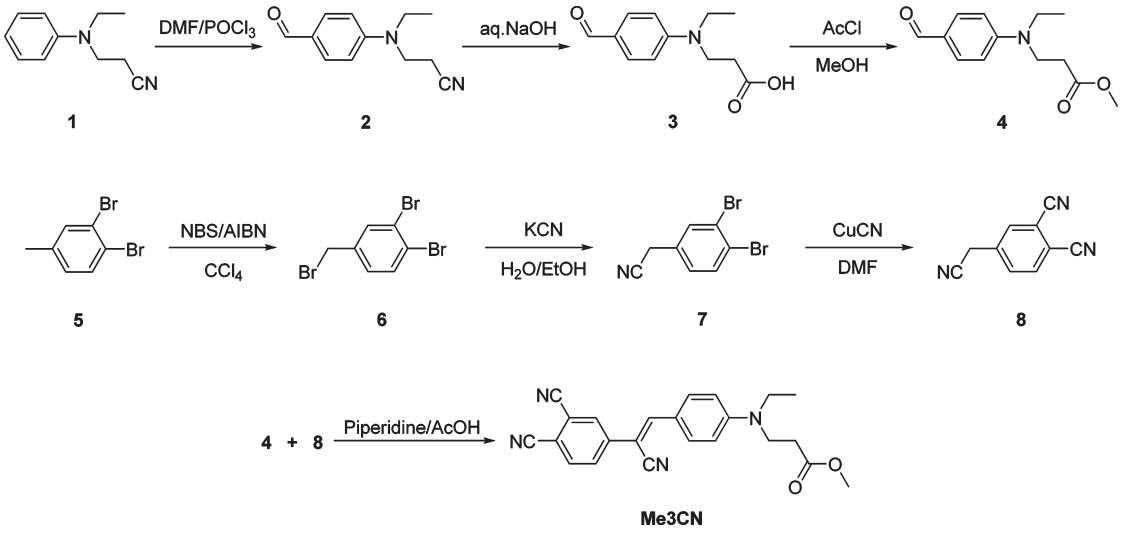

occurring in α-cyanostilbenes.[10b,g] Overall, nanoaggregates of Me3CN emit enhanced reddish fluorescence with a considerable component in the NIR, useful for bioimaging applications. The Me3CN emission could be moved even further toward the NIR by changing the way of assembly, that is, from nanoaggregation to solution- or melt-crystallization, as shown in Figure 2c as well as discerned by different fluorescence colors in Figure 2a. Powder X-ray diffraction data of solution- and melt-grown crystals suggests that the variation of fluorescence is governed by the distinct crystal structures (Figure 2d). This implies that the fluorescence of AIEE dye aggregates can be tuned with dual controllability by engineering the molecular structures as well as the crystalline packing modes, offering a promising methodology to fabricate advanced NIR nanoprobes.

Dye-integrated biopolymeric amphiphiles (GC3CN*x*) were synthesized by amidation between carboxylic 3CN and free amines of GC in DMSO/water, in the presence of 1-ethyl-3-(3-dimethylaminopropyl) carbodiimide

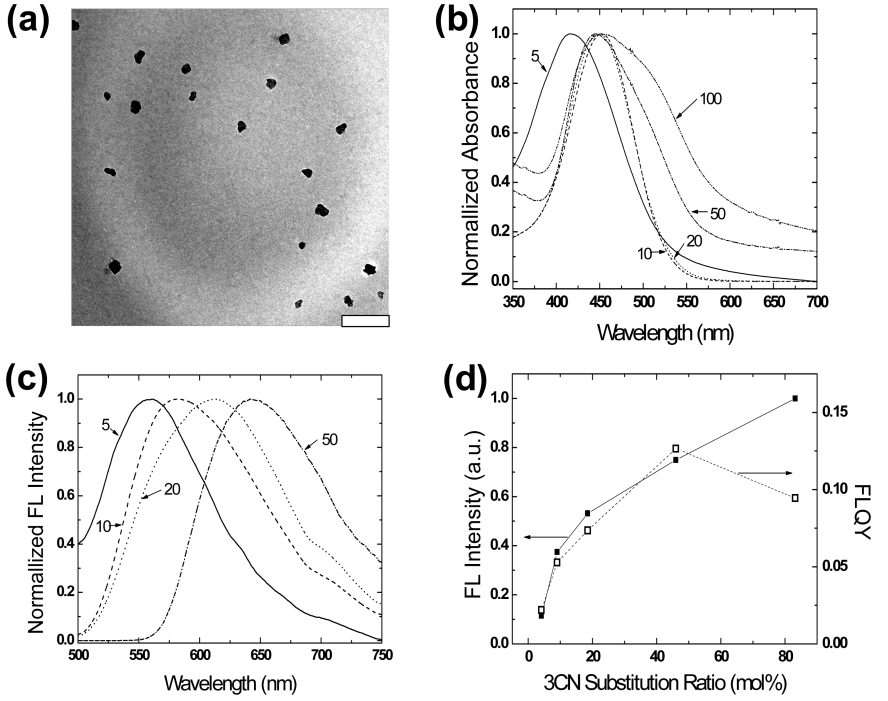

Figure 3. (a) TEM image of GC3CN50 nanoparticles. The scale bar presents 200 nm. (b) and (c) Normalized absorption and FL spectra of GC3CN*x* nanoparticles dispersed in water (1 mg mL^{-1}), respectively. The 3CN feed ratio in GC3CN*x* is indicated by numbers in mol % (x = 5, 10, 20, 50, and 83%). (d) Evolution of the total fluorescence output (■) and quantum yield (□) from water-dispersed GC3CN*x* nanoparticles (1 mg mL^{-1}), as a function of 3CN substitution ratio. The quantum yields were relatively determined with Rhodamine B as a reference.

hydrochloride (EDC) and *N*-hydroxysuccinimide (NHS) (Figure 1). The feed amount of 3CN was varied to assess the effect of dye concentration on the AIEE behavior of self-assembled GC3CN*x* nanoparticles, where *x* indicates the feed ratio of 3CN (mol %) against all repeating units of GC in the coupling reaction. The mild reactions at ambient temperature for 24 h afforded the GC3CN *x* polymers with 4.1, 9.0, 18.5, 46.0, and 83.2 mol % substitution ratios, respectively. The purification was conducted by dialyzing the reaction mixtures against DMSO and then the medium was exchanged into an aqueous milieu by subsequent dialysis against excess pure water. During the latter step, all the GC3CN*x* amphiphiles formed stable dispersions of self-assembled nanoparticles in water with hydrodynamic diameters of 200−400 nm, as determined by dynamic light scattering (DLS) (see SI Table S1). It was found that the lyophilized GC3CN*x* nanoparticles can be redispersed in water by sonication except highly substituted GC3CN50 and GC3CN83. Transmission electron microscopy (TEM) of unstained GC3CN50 nanoparticles showed high-electron-density domains with irregular shapes (< 60 nm), most probably indicative of the aggregated hydrophobic cores of the π-electron-rich 3CN units inside the invisible GC outer shells (Figure 3a).

The evolution of optical properties with increasing feed ratio suggests that the particulate self-assembly of GC3CN*x* is unambiguously attributed to the cooperative hydrophobic and $\pi-\pi$ interactions between the chromophoric pendants, that is, the fluorescence-enhancing aggregation of the 3CN units. As shown in the absorption and fluorescence spectra of GC3CN*x* nanoparticles (Figure 3b and c), gradual red shifts and/or increased contributions of longer-wavelength components were observed with higher substitution of 3CN. This means that the degree of dye substitution governs the balance between the interpendant attraction and the free motion of GC backbone. The resulting nanoscopic structure would in turn determine the spectral characteristics in a way that the higher substitution causes the more red-shifted emission through the closer packing of the planar 3CN pendants, similar to the AIEE behavior of Me3CN that depends on the molecular stacking modes. Importantly, the total fluorescence output from the same amount of the bionanoparticles was increased by raising the 3CN substitution even up to the maximum (Figure 3d), which is directly opposed to concentration quenching of common organic dyes in nanoparticles.[8a] This behavior is exactly consistent with that of the quantum yield (Figure 3d), only except a deviation of GC3CN83. The quantum yield drop of GC3CN83 is likely an artifact originated from the raised value of absorbance due to the scattering-induced baseline offset (Figure 3b). The severe scattering of the GC3CN83 nanoparticles is attributable to the biggest size as well as to the probably highest refractive index due to the wealth of π-electrons. The initial jumps in the FL intensity and quantum yield indicate that the 3CN pendant aggregation becomes pronounced above 10% feeding, well accordant with an abrupt shift of the absorption peak from 420 nm (GC3CN5) to 450 nm (GC3CN10). The same maximum wavelength with an increasing longer-wavelength shoulder, in the absorption spectra above 10% feeding, might be attributed to the presence of multiple

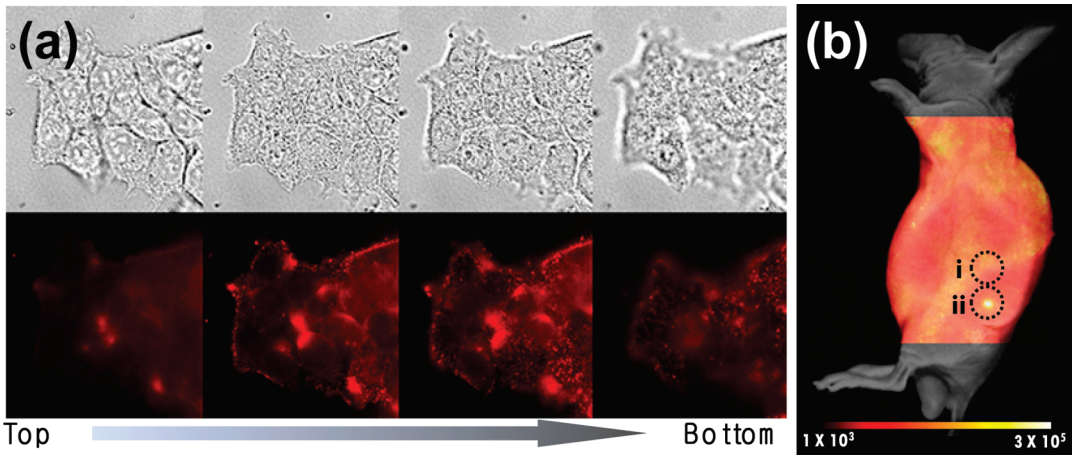

Figure 4. Cellular and in vivo imaging with GC3CN*x* nanoparticles. (a) *Z*-axis scanned optical (upper) and pseudocolored NIR fluorescence (lower) images from top (left) to bottom (right) of HeLa cells treated with water-dispersed GC3CN20 nanoparticles. (b) Overlay views of optical (gray) and pseudocolored NIR fluorescence (colored) images of a live mouse subcutaneously injected with nanoparticle dispersions of (i) GC3CN20 and (ii) GC3CN50.

absorbing species: the highest-energy aggregates are the majority and the relative amount of lower-energy species increases gradually with the dye concentration. The gradual emission shift, compared to the limited changes in the absorption spectra above 10% feeding, suggests the energy funneling to the aggregates of the lowest excited state through intraparticle energy transfer. Overall, a simple increase in the dye substitution from 5 to 83% feeding offered NIR-active bionanoparticles useful for bioimaging, with a remarkable emission shift toward the NIR and 9-fold enhancement of the signal intensity as well as sustained colloidal stability in water.

To evaluate the utility of dye-concentrated bionanoparticles for imaging applications, we explored fluorescence imaging experiments in cells and in vivo. For tumor cell imaging, HeLa (human cervical epitheloid carcinoma) cells were incubated with GC3CN20 nanoparticles and observed under the NIR-filtered fluorescence microscope. After 2 h of incubation at 37 °C, the nanoparticle-treated cells showed clear NIR fluorescence in the cytoplasmic regions (Figure 4a). This avid cellular uptake indicates that the biopolymeric surface properties of the hybrid nanoparticles facilitates their internalization into cells by several nondestructive endocytic pathways that are operative in GC-based nanoparticles.[13d] To our interest, in vivo imaging demonstrated more markedly the merits of the concentrated dye integration in GC3CN nanoparticles. When GC3CN20 and GC3CN50 nanoparticles were subcutaneously injected to the side of a live mouse, the signal contrast between them were clearly observed in a NIR imaging system equipped with a Cy5.5 emission filter (680−720 nm) (Figure 4b). It was estimated that the in vivo signal from the GC3CN50 spot is 35 times intenser compared to GC3CN20, although their in vitro intensity shows only 1.4-fold difference (Figure 3d). This remarkable signal improvement under in vivo condition is ascribed to the AIEE characteristics of GC3CN nanoparticles, that is, the concentration-promoted dye aggregation and thus the enhanced and NIR-shifted fluorescence thereby (Figure 3c and d). It should be noted that the NIR-shifted signal has better penetration through the skin as well as better spectral coincidence with the detection window of common NIR imaging equipments. These data demonstrate the significance of NIR photonics for bioimaging, validating our present AIEE-based approach toward NIR nanoprobes.

3. Conclusion

We have designed and prepared a new AIEE-active α-cyanostilbene derivative (Me3CN) and biopolymeric amphiphiles densely integrated therewith (GC3CN*x*) to take combined advantages of photonic and biologically functional materials. The obtained amphiphilic GC3CN*x* showed supramolecular self-assembly behavior into stably dispersed nanoparticles in an aqueous milieu, driven by fluorescence-enhancing aggregation of 3CN pendants. It has been shown that higher dye substitution into the glycol chitosan backbone renders the fluorescence of the self-assembled nanoparticles intenser and more red-shifted toward the NIR. Cellular and in vivo imaging experiments have demonstrated the potentials of aggregation-enhanced NIR fluorescence and AIEE-implemented hybrid bionanoparticles for bioimaging applications.

4. Experimental Section

4.1. Instrumentation. ^{1}H NMR measurements were recorded on a Avance DPX-300 (300 MHz, Bruker, Germany) in $CDCl_3$, DMSO-d_6, and aceton-d_6 solution. The data of elemental analysis were measured on EA1110 (CE Instrument, Italy). UV−visible absorption and fluorescence spectra were measured on a 8453 UV−visible spectrophotometer (Agilent Technology, U.S.) and a F-7000 fluorescence spectrophotometer (Hitachi, Japan), respectively. Dynamic light scattering (DLS) measurement was carried out at 633 nm (Spectra Physics laser model 127-35). The intensity autocorrelation of the sample was measured at a scattering angle of 90° with a BI-9000AT digital autocorrelator (Brookhaven, NY). Powder X-ray diffractograms were taken with General Area Detector Diffraction System (GADDS, Bruker) at Cu Kα radiation.

4.2. Synthesis of 3-(Ethyl-(4-formylphenyl)-amino)-propanenitrile (2). Dimethylformamide (DMF, 26.5 mL, 342 mmol) was stirred in ice bath, then $POCl_3$ (15.8 mL, 171 mmol) was added dropwise. After 1 h, **1** (10 g, 57 mmol) was added to the solution and the solution was refluxed at 100 °C for 1 h. Sodium bicarbonate and ice was added to the solution, then extracted with ethyl acetate five times. The organic layer was dried with magnesium sulfate and solvent was evaporated. The residue was purified by column chromatography on silica gel with ethyl acetate/*n*-hexane (1/5) to give **2** (yield: 8.47 g, 68%). ^{1}H NMR (300 MHz, $CDCl_3$) δ ppm]: 9.79 (s, 1H), 7.76 (d, 2H), 6.72 (d, 2H), 3.74 (t, 2H), 3.58 (q, 2H), 2.69 (t, 2H), 1.20 (t, 3H).

4.3. Synthesis of 3-(Ethyl-(4-formylphenyl)-amino)-propanoic acid (3). A mixture of **2** (5 g, 25 mmol) and sodium hydroxide (2 g, 50 mmol) in water (100 mL) was refluxed until the nitrile layer disappears (10 h). We added 50 mL of water through the condenser, and 3 mL of 50% sulphuric acid was added slowly with external cooling. The mixture was extracted three times with ethyl acetate and the organic layer was dried with magnesium sulfate. The product was purified by extraction in acidic and basic condition to give **3** (yield: 4.55 g, 83%). ^{1}H NMR (300 MHz, Aceton-d_6) δ ppm]: 9.71 (s, 1H), 7.72 (d, 2H), 6.86 (d, 2H), 3.76 (t, 2H), 3.59 (q, 2H), 2.68 (t, 2H), 1.20 (t, 3H).

4.4. Synthesis of Methyl 3-(ethyl-(4-formylphenyl)-amino)-propanoate (4). A solution of **3** (2.5 g, 11 mmol) in methanol (50 mL) was stirred, then acetyl chloride (4.1 mL, 55 mmol) was added dropwise. The solution was refluxed for 4 h, and then the solution was basified with concentrated potassium carbonate with external cooling. The solution was extracted three times with methylene chloride, and the organic was dried with magnesium sulfate. The product was purified by column chromatography on silica gel with ethyl acetate/*n*-hexane (1/2) to give **4** (yield: 2.4 g, 90%) ^{1}H NMR (300 MHz, $CDCl_3$) δ ppm]: 9.73 (s, 1H), 7.76 (d, 2H), 6.73 (d, 2H), 3.72 (t, 2H), 3.70 (s, 3H), 3.48 (q, 2H), 1.20 (t, 3H).

4.5. Synthesis of 1,2-Dibromo-4-(bromomethyl)-benzene (6). Compound **5** (25 g, 100 mmol) and *N*-bromosuccinimide (17.8 g, 100 mmol) were dissolved in carbon tetrachloride, and 2, 2′-azobisisobutyronitrile (AIBN) (0.165 g, 1 mmol) was added to the solution, and then the solution was refluxed at 80 °C for 8 h. To the solution cooled to room temperature was added 500 mL of aqueous $NaHCO_3$, and then the mixture was stirred at room temperature for 2 h. The solution was extracted with chloroform and dried by evaporation. The product was purified by column chromatography on silica gel with *n*-hexane to give **6** (yield: 29.6 g, 91%). ^{1}H NMR (300 MHz, $CDCl_3$) δ ppm]: 7.65 (s, 1H), 7.57 (d, 1H), 7.19 (d, 1H), 4.38 (S, 2H).

4.6. Synthesis of 2-(3,4-Dibromophenyl)-acetonitrile (7). Compound **6** (25.7 g, 78.2 mmol) and KCN (7.63 g, 117.2 mmol) were dissolved in water/ethanol (1/3 by vol.), and the solution was refluxed at 88 °C for 12 h. The mixture was extracted with ethyl acetate, and dried with magnesium sulfate, and then the solvent was evaporated. The product was purified by column chromatography on silica gel with ethyl acetate/*n*-hexane (1/3) to give **7** (yield: 8.1 g, 38%). ^{1}H NMR (300 MHz, $CDCl_3$) δ ppm]: 7.61−7.65 (m, 2H), 7.14 (d, 1H), 3.17 (s, 2H).

4.7. Synthesis of 4-(Cyanomethyl)-phthalonitrile (8). Compound **7** (2 g, 7.2 mmol) and CuCN (2.6 g, 29 mmol) were dissolved in anhydrous DMF, and the solution was refluxed at 150 °C for 4 h. The solution was cooled to room temperature, and extracted with ethyl acetate 2 h. The solution was filtered, and the filtrate was washed with aq. NH_4Cl solution. The organic layer was dried with magnesium sulfate, and the solvent was evaporated. The product was purified by column chromatography on silica gel with ethyl acetate/*n*-hexane (1/1) to give **8** (yield: 0.25 g, 21%). ^{1}H NMR (300 MHz, $CDCl_3$) δ ppm]: 7.86 (d, 1H), 7.81 (s, 1H), 3.91 (s, 2H).

4.8. Synthesis of (Z)−Methyl 3-((4-(2-cyano−2-(3,4-dicyanophenyl)vinyl)phenyl)-ethyl-amino)-propanoate (Me3CN). Compounds **4** (155 mg, 0.66 mmol) and **8** (100 mg, 0.60 mmol) were dissolved in acetonitrile (6 mL), and the solution was stirred under nitrogen flow at room temperature. Five drops of piperidine and acetic acid were added to the solution, and the reaction mixture was stirred in the dark at room temperature for 15 h. The solvent was evaporated to give red powder. The powder was recrystallized in methanol to give **9** (yield: 207.7 mg, 90%). ^{1}H NMR (300 MHz, $CDCl_3$) δ ppm]: 8.02 (d, J = 1.88, 1H), 7.94(dd, J = 8.10, 1.95, 1H), 7.92 (d, J = 8.78, 2H), 7.82 (d, J = 8.35, 2H), 7.51 (s, 1H), 6.73 (d, J = 9.09, 2H), 3.74 (t, J = 7.13, 2H), 3.72 (s, 3H), 3.51 (q, J = 7.09, 2H), 2.67 (t, J = 7.46, 2H), 1.23 (t, J = 7.01). ^{13}C NMR (75 MHz, $CDCl_3$) δ ppm]: 171.895, 150.430, 146.010, 141.136, 133.938, 132.984, 129.425, 129.024, 120.318, 118.081, 116.639, 115.324, 115.137, 113.388, 111.585, 99.460, 51.963, 46.047, 45.339, 32.300, 12.337. anal. calcd for $C_{23}H_{20}N_4O_2$: C 71.86, H 5.24, N 14.57; found: C 71.86, H 5.23, N 14.53.

4.9. Synthesis of (Z)−3-((4-(2−cyano−2-(3,4-dicyanophenyl)-vinyl)phenyl)-ethyl)-amino)-propanoic acid (3CN). Me3CN (100 mg, 0.26 mmol) was dissolved in THF (12 mL) at 40 °C, and 4 mL of aq. lithiumhydoxide monohydrate (109 mg, 2.6 mmol) solution was added dropwise, and then the reaction mixture was stirred in the dark at 40 °C for 30 min. The mixture was poured into water and acidified with HCl until pH 2. The product was extracted with ethyl acetate, and the organic layer was dried with magnesium sulfate, and then the solvent was evaporated. The residue was dissolved in acetone, and the product was reprecipitated three times into cyclohexane to give 3CN (yield: 40 mg, 42%) ^{1}H NMR (300 MHz, Aceton-d_6) δ ppm]: 8.36 (d, J = 1.56, 1H), 8.16 (dd, J = 8.37, 1.89, 1H), 8.14 (d, J = 8.16, 2H),8.09 (s, 1H), 8.02 (d, J = 9.09, 2H), 6.92 (d, J = 9.18, 2H), 3.80 (t, J = 7.08, 2H), 3.62 (q, J = 7.02, 2H), 2.70 (t, J = 7.38, 2H), 1.23 (t, J = 7.05). ^{13}C NMR (75 MHz, Aceton-d_6) δ ppm]: 173.089, 151.718, 147.614, 142.319, 135.363, 133.835, 130.498, 130.439, 121.541, 119.056, 117.164, 116.587, 116.454, 113.881, 112.623, 99.968, 46.794, 45.839, 32.651, 12.648. anal. calcd for $C_{22}H_{18}N_4O_2$: C 71.34, H 4.90, N 15.13; found: C 71.36, H 4.94, N 15.19.

4.10. Preparation of GC3CN*x* Amphiphiles and Nanoparticles Thereof. Glycol chitosan (GC, M_W = 250 kDa; degree of deacetylation = 82.7%; Sigma) (25 mg, 0.122 mmol (unit)) was dissolved in 2 mL of distilled water with sonication and a DMSO (10 mL) solution containing 3CN, 1-ethyl-3-(3-dimethylaminopropyl) carbodiimide hydrochloride (EDC) and *N*-hydroxysuccinimide (NHS) was added. The molar ratio (x) of 3CN feed was 5, 10, 20, 50, and 83% with respect to the total GC repeating unit. For each GC3CNx, 1.5 times excess molar coupling agents (EDC and NHS, respectively) with respect to the 3CN feed were introduced, then the reaction mixtures were stirred at ambient temperature for 24 h. To quantify of the substitution ratios, the reaction mixtures (200 μL) were mixed with THF (800 μL) and centrifuged, to obtain precipitates of GC-3CN conjugates. The substitution ratios were indirectly determined through the measurements of the unreacted free 3CN concentration in the supernatants of the centrifuged mixtures by UV absorbance-based quantification. For the further applications, the coupling reaction mixtures were subjected to the successive dialysis against DMSO (2 days) and water (2 days) using a Cellu·Sep membrane (Membrane Filteration Products, Inc., molecular cutoff = 50 kDa). The resulting dispersions of nanoparticles were freeze-dried or used as is for characterization and imaging

experiments. The dried GC3CN*x* with low substitution ($x = 5$, 10, and 20) were able to be redispersed in water at 1 mg mL^{-1} under probe sonication at 90 W for 2 min (Sigma Ultrasonic Processor, GEX-600). All the dried GC3CN*x* were not able to be redissolved in DMSO or relevant solvents for NMR measurement and other solution characterizations.

4.11. Cellular Uptake Assay. HeLa cells were plated on a 35 mm culture dishes at a density of 1×10^5 cells/well and cultured with GC3CN20 nanoparticles (0.2 mg mL^{-1}) for 2 h at 37 °C. After incubation, the cells were washed with PBS (1 mL × 2, pH 7.4) to remove free nanoparticles. Cellular images were acquired with Deltavision-RT system (Applied Precision, Inc. Issaquah, WA) using an IX71 inverted microscope (Olympus, Tokyo, Japan) and a filter set of TRITC exitation/Cy5.5 emission.

4.12. In Vivo Imaging. All handling of mice was in accordance with the regulations of Korea Institute of Science and Technology. For animal experiments, a BALB/c nude mouse (male, 8 weeks of age; Institute of Medical Science, Tokyo) was initially anaesthetized with intraperitoneal injection of 0.5% pentobarbital sodium (0.10 mL/10 g) and subcutaneously injected with GC3CN20 and GC3CN50 nanoparticle dispersions (10 μL, 1 mg mL^{-1}). The in vivo imaging experiment was conducted with 12-bit CCD camera (Kodak Image Station 4000MM, New Haven, CT) equipped with a special C-mount lens. The NIR image was obtained with a filter set of TRITC for exitation and Cy5.5 for emission (680−720 nm; Omega Optical).

Acknowledgment. This work was supported by the Creative Research Initiative Program (0417-20090011) and the Real-Time Molecular Imaging Project funded by the Korea Ministry of Education, Science and Technology (MEST) and by the Intramural Research Program of KIST.

Supporting Information Available: Table S1 and Figure S1 (PDF). This material is available free of charge via the Internet at http://pubs.acs.org.